BIOCHEMISTRY
including biophysical chemistry & molecular biology

Article

pubs.acs.org/biochemistry

Spontaneous Rearrangement of the β20/β21 Strands in Simulations of Unliganded HIV-1 Glycoprotein, gp120

Indira H. Shrivastava,*[,†] Kaylee Wendel,[‡] and Judith M. LaLonde[‡]

[†]Department of Systems and Computational Biology, School of Medicine, University of Pittsburgh, 3089 Biomedical Science Tower 3, 3501 Fifth Avenue, Pittsburgh, Pennsylvania 15213, United States

[‡]Chemistry Department, Bryn Mawr College, 101 N. Merion Avenue, Bryn Mawr, Pennsylvania 19010, United States

Supporting Information

ABSTRACT: Binding of the viral spike drives cell entry and infection by HIV-1 to the cellular CD4 and chemokine receptors with associated conformational change of the viral glycoprotein envelope, gp120. Crystal structures of the CD4−gp120−antibody ternary complex reveal a large internal gp120 cavity formed by three domains—the inner domain, outer domain, and bridging sheet domain—and are capped by CD4 residue Phe43. Several structures of gp120 envelope in complex with various antibodies indicated that the bridging sheet adopts varied conformations. Here, we examine bridging sheet dynamics using a crystal structure of gp120 bound to the F105 antibody exhibiting an open bridging sheet conformation and with an added V3 loop. The two strands of the bridging sheet β2/β3 and β20/β21 are dissociated from each other and are directed away from the inner and outer domains. Analysis of molecular dynamics (MD) trajectories indicates that the β2/β3 and β20/β21 strands rapidly rearrange to interact with the V3 loop and the inner and outer domains, respectively. Residue N425 on β20 leads the conformational rearrangement of the β20/β21 strands by interacting with W112 on the inner domain and F382 on the outer domain. An accompanying shift is observed in the inner domain as helix α1 exhibits a loss in helicity and pivots away from helix α5. The two simulations provide a framework for understanding the conformational diversity of the bridging sheet and the propensity of the β20/β21 strand to refold between the inner and outer domains of gp120, in the absence of a bound ligand.

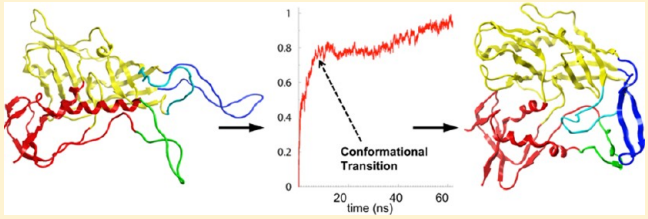

Infection of HIV-1 begins with a series of dynamic binding events between the trimeric glycoprotein envelope spike and the host cell CD4 and chemokine receptors.[1−7] The envelope trimer (gp160) is composed of three gp120 glycoproteins and three transmembrane gp41 proteins.[8−10] The first dynamic event occurs via binding of gp120 to the host T-cell CD4 receptor[3,11] followed by extensive restructuring of gp120.[12,13] This conformational change results in the exposure of the chemokine binding site on gp120, thus permitting binding to either of the chemokine receptors, CCR5 or CXCR4.[14−17] Upon chemokine receptor binding a second conformational change occurs in gp41 to form the fusion peptide that inserts in the host cell membrane, leading to viral entry.[6,18−20] The CD4 induced gp120 conformational change has been characterized thermodynamically, showing a highly favorable binding enthalpy balanced with a highly unfavorable molecular ordering.[21,22] This thermodynamic signature resembles protein folding, rather than binding, and reflects the large molecular ordering of gp120 upon CD4 binding.[21] A similar thermodynamic signature is exhibited by soluble CD4 (sCD4) binding to both full-length gp120 ($gp120_{full}$) and a core gp120 ($gp120_{core}$) containing truncations in gp120 variable loops.[22−24] Furthermore, the large entropic penalty associated with CD4 binding was substantially reduced for a cavity filling mutant (S375W), indicating that this mutant gp120 is stabilized in a CD4 bound-like state.[25,26]

There are several $gp120_{core}$ structures bound with CD4 receptor,[27−31] antibodies,[32−35] miniprotein,[36,37] and small molecule ligands[38,39] detailing gp120−ligand interactions. The CD4−$gp120_{core}$ crystal structures reveal the CD4 induced formation of a large internal gp120 cavity formed by the inner, outer, and bridging sheet domains (the CD4 bound conformation of gp120 is denoted as $gp120_{CD4}$) (Figure 1A).[27,28] The highly conserved CD4 Phe43 side chain binds at the top of the gp120 "Phe43 cavity". The structure of the biphenyl conjugated scyllatoxin derived mini-protein (2I5Y)[36] reveals the depth of the cavity and biphenyl interactions with gp120 aromatic residues lining the Phe43 cavity from each of the three domains, namely, W112 (inner domain) F382 and Y384 (outer domain), and W427 (bridging sheet). In $gp120_{CD4}$, the bridging sheet domain is composed of a four-stranded antiparallel β-sheet (β2, β3, β20, β21). The β2/β3 strands stem from the inner domain, while the β20/β21 strands arise from the outer domain. Thus, the bridging sheet spans the interface of both the inner and outer domain and forms a third of the surface of the Phe43 cavity. As yet, structural information on the prestructured, unbound form of trimeric gp120 has been elusive. However, the structure of the unbound form of SIV

Received: June 29, 2012
Revised: September 6, 2012
Published: September 10, 2012

ACS Publications © 2012 American Chemical Society

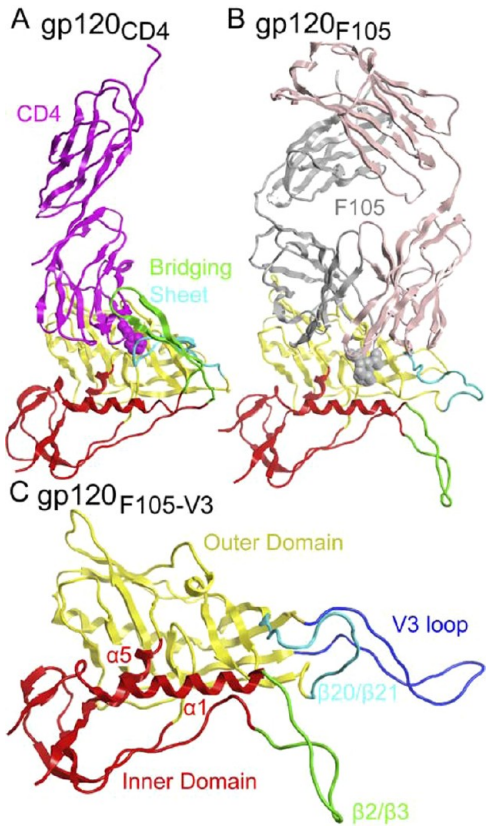

Figure 1. Conformations of gp120. (A) The CD4 (magenta) bound conformation of gp120 ($gp120_{CD4}$). The CD4 residue Phe43 (magenta spheres) binds atop a large internal cavity (the "Phe43 cavity") formed by the inner domain (red), outer domain (yellow), and the bridging sheet composed of the $\beta2/\beta3$ strands (green) and the $\beta20/\beta21$ strands (cyan). The crystal complex 1G9N also contains the chemokine antibody surrogate, 17b, which is not shown here. (B) The F105 antibody (gray and pink) bound conformation of gp120 ($gp120_{F105}$). The F105 Val-Phe-Tyr motif (gray spheres) binds a shallower and more open "Phe43 cavity". The $\beta2/\beta3$ strands (green) and the $\beta20/\beta21$ strands (cyan) are extended away from the Phe43 cavity and disassociated. (C) The $gp120_{F105-V3}$ model used in MD simulations contains the V3 loop (dark blue) grafted onto $gp120_{F105}$.

gp120 has been solved, revealing a structurally invariant outer domain with a markedly different conformation and arrangement of the inner domain and bridging sheet domains compared to HIV-1 $gp120_{CD4}$ structures.[40] In fact, the structure of $gp120_{CD4}$-containing portions of the gp41-interacting region displays a three-layered domain architecture adjacent to the invariant outer domain.[31] This topological layering of the gp41-interacting elements, the inner domain, and bridging sheet domain is postulated to form a "shape-changing spacer" that forms the basis of glycoprotein conformational mobility.[31,41] The plasticity of monomeric $gp120_{core}$ in complex with several monoclonal antibodies, b12 (2NY7),[29] b13 (3IDX), and F105 (3HI1),[32] and the N-terminal of the CCR5 receptor (2QAD)[42] also reveal the structural variability of the inner domain, bridging sheet, and variable loops.[43] The structure of tyrosine-sulfated 412d antibody complexed with HIV-1 YU2 gp120 and CD4, reveals the structure of the V3 loop situated adjacent to the bridging sheet (2QAD).[42] The gp120 bound N-terminal of the CCR5 receptor (2QAD), which is the structure of tyrosine-sulfated 412d antibody complexed with HIV-1 YU2 gp120, and CD4, reveals the structure of the V3 loop situated adjacent to the bridging sheet. This highly variable, glycosylated, 35-residue V3 loop determines HIV-1 trimer preference for binding to either the CCR5 or CXCR4 chemokine receptors.[44−46] Furthermore, Yokoyama et al. found that the V3 loop acts as an electrostatic modulator that impacts the fluctuation and conformation of CD4, coreceptor, and antibody binding loops.[47] Other disulfide bond linked $gp120_{core}$ variants complexed to b12 and b13 display an altered conformation compared to the CD4-bound state with shifts in the V1/V2 stem and alternations in the position and orientation of the bridging sheet $\beta2/\beta3$ and $\beta20/\beta21$ strands. Furthermore, the b12−$gp120_{core}$ complex displays an unstructured helix $\alpha1$ in the inner domain. This is in contrast to the F105−$gp120_{core}$ ($gp120_{F105}$) complex (Figure 1B), which shows a structured helix $\alpha1$, but with narrowing of the interface between the inner domain and outer domain. This narrowing is accompanied by the displacement and disassociation of the 30 residues of the four-stranded antiparallel β-sheet bridging sheet into distinct conformations for the $\beta2/\beta3$ and $\beta20/\beta21$ strands. The two strands extend away from the inner−outer domain interface, resulting in a shallower and more open "Phe43 cavity" bound by the F105 antibody Val-Phe-Tyr motif (Figure 1B). Thus, these antibody-stabilized complexes represent gp120 conformations that may be sampled along the transition path between the unliganded and the CD4 bound form. Recently, Kwon et al. have solved the structure of the unliganded gp120 extended core ($gp120_{coreE}$) from clades B, C, and E and demonstrate that while the glycoprotein trimer spike rarely assumes a CD4-bound like conformation, $gp120_{coreE}$ spontaneously adopts the CD4 bound conformation in the absence of ligand when not restricted by the presence of the V1, V2, and V3 variable loops.[38] Therefore, ligand binding is not a prerequisite for the creation of the $gp120_{CD4}$ conformation, suggesting that this conformation may indeed be sampled in solution in the context of the $gp120_{core}$.

The conformational dynamics of gp120 has been analyzed using various computational models reiterating the bridging sheet flexibility seen in gp120-antibody crystal structures. Floppy Inclusion and Rigid Substructure Topography analysis of several gp120 structures bound with various ligands demonstrated that the inner domain and bridging sheet domains are more flexible while the outer domain is more rigid.[48] Several simulations of gp120 bound with CD4, miniprotein, or small molecule using the coarse-grained Gaussian network model also concluded that the outer domain was more rigid and exhibited less flexibility than the inner domain and the bridging sheet.[49] Application of temperature accelerated MD predicted a counter rotation between the inner and outer domains and a disruption of the bridging sheet in the unbound form of gp120.[50] Additional MD studies by Hsu et al. indicate that there are concerted loop motions in the vestibule of the CD4 cavity, stabilization of the bridging sheet, and a coalescing of the bridging sheet and V3 loop to form the coreceptor binding site.[51,52] MD studies demonstrated that the bridging sheet refolds for a S375A mutant,[53] while the bridging sheet did not refold for either a S375W cavity mutant[54] or double mutant, S375W/T257.[53] Furthermore, Liu et al. showed that a gp120 homology model containing the S375W mutation favors the CD4 bound conformation, while the I423P mutation prefers an unliganded conformation.[55] Nonequilibrium steered MD showed that the bridging sheet strands $\beta2/\beta3$ had more flexibility than the $\beta20/\beta21$ strands, which preferred interactions with the inner domain.[56] MD simulation of

gp120 showed that the binding of the small molecule, NBD-556, within the Phe43 cavity enhances the dynamics of gp120 with increased mobility, especially in the outer domain, as compared to the CD4 bound or miniprotein bound complex.[57] More recently, Yokoyama et al. describe MD simulations of gp120 in the CD4 bound form containing the V3 loop, concluding that the V3 loop acts as an electrostatic modulator that impacts the fluctuation and conformation of CD4, coreceptor, and antibody binding loops.[47]

The thermodynamic, crystallographic, and dynamic studies all suggest that gp120 is in equilibrium among a number of conformational states, which when bound by ligand (CD4, antibody, miniprotein, or small molecule) can drive the equilibrium toward a conformational state that favors binding to the chemokine coreceptor. However, the molecular mechanism of the transition between these conformational states remains undetermined. Nonetheless, as revealed by the CD4−gp120 structure containing portions of the gp41-interacting region[31] and the $gp120_{F105}$ structure (3HI1),[32] the inner domain and bridging sheet are most likely to facilitate/mediate conformational changes compared to the outer domain, which has thus far been observed in a conserved conformation. We postulate that the extended conformations of the $\beta2/\beta3$ and $\beta20/\beta21$ as observed in the $gp120_{F105}$ structure represent one potential conformation of the metastable unliganded gp120 monomer. Moreover, the observation that the unliganded $gp120_{coreE}$ adopts the $gp120_{CD4}$ conformation without induction by ligand binding suggested further investigation of interdomain interactions that may contribute to gp120 conformational transitions. In this study, we use MD simulations to explore the conformational rearrangement of the bridging sheet as observed in the unliganded $gp120_{F105}$ structure containing the V3 loop. The two 100 ns simulations reported herein demonstrate that the $\beta2/\beta3$ and $\beta20/\beta21$ strands and the V3 loop rearrange spontaneously, leading to reorganization of the $\beta20/\beta21$ strand wedged between the inner domain and outer domain accompanied by a shift in the position of helix $\alpha1$ on the inner domain.

MATERIALS AND METHODS

For this study, we used the crystal structure of YU2 gp120-core complexed to the F105-antibody (3HI1).[32] The conformation of the third variable loop (V3) was revealed in the crystal structure of the gp120 complexed to the tyrosine-sulfated 412d antibody (2QAD).[43] Superposition of the outer domain of these two structures indicated that the V3 loop could be grafted onto the V3 stem in the outer domain of 3HI1 without disrupting the extended position of the bridging sheet strands $\beta20/\beta21$. Using the homology modeling module in MOE,[58] the V3 loop from 2QAD was grafted onto the corresponding YU2 sequence in context of the 3HI1 structure. This loop was added to provide completeness to the monomer structure and to assess the role of adjacent V3 loop on bridging sheet dynamics. The missing residues corresponding to the V4 loop in 3HI1 were added from the 1G9N[27] crystal structure, and the resulting structure was energy minimized. Hydrogen atoms were added, and the tautomeric states and orientations of Asn, Gln, and His residues were determined with MolProbity.[59,60] The construct was then minimized using the OPLS-AA force field[61] in MOE[58] with the following procedure: all hydrogen atoms were minimized to a root-mean-square (rms) gradient of 0.01, holding the heavy atoms fixed. A stepwise minimization followed for all atoms, using a quadratic force constant (100 kcal mol^{-1} $Å^{-1}$) to tether the atoms to their starting geometries; for each subsequent minimization, the force constant was reduced by a half until 0.25 kcal mol^{-1} $Å^{-1}$. This was followed by a final cycle of unrestrained minimization. Water molecules, Asn-linked acetyl-D-glucosamine, 2-(acetylamino)-2-deoxy-α-D-glucopyranose, and small molecules were removed prior to MD calculations.

Molecular Dynamics Simulations. The model of gp120, including the bridging sheet and the V3 loop, in explicit solvent, was initially energy minimized, using the steepest descent algorithm, in GROMACS software.[62] This energy-minimized model included explicit SPC[63] water molecules, resulting in a simulation model of ∼55 000 atoms. After energy minimization, the system was equilibrated for 1 ns, during which the backbone atoms were restrained by a harmonic potential of 1000 kJ mol^{-1} nm^{-1}, while the side-chain atoms and the water molecules were allowed to relax. This was then followed by a production run of 100 ns, during which all restraints were removed. The simulations were all performed under constant number of particles, pressure, and temperature conditions with temperature set at 310 K. A weak temperature coupling using Berendsen's bath with a time constant of 0.1 ps was used, while a pressure coupling of 1 atm/bar with a time constant of 1 ps was applied, also using the Berendsen's algorithm.[64] The LINCS algorithm[65] was used to constrain bonds involving hydrogen atoms, and the integration time step was set to 2 fs. The electrostatic interactions were calculated using Ewald particle mesh method.[66] Two 100 ns simulation trajectories were generated from this energy-minimized and equilibrated system each started off with a different set of random initial velocities. In the following discussion, these will be denoted as MD-1 and MD-2. The simulation trajectories were all generated on the supercomputing resources available at the Pittsburgh Center for Simulation and Modeling.

RESULTS AND DISCUSSION

gp120 Exhibits a Conformational Transition after 40 ns of Simulation. The unliganded monomer gp120 core extracted from the 3HI1 complex[32] was used for simulations. The V3 loop was grafted from the gp120−412d antibody structure (2QAD)[43] to provide completeness to the gp120 monomer structure ($gp120_{F105-V3}$) and to assess its impact on bridging sheet dynamics, Figure 1 (see Materials and Methods). Two 100 ns simulations were conducted for $gp120_{F105-V3}$ and are denoted MD-1 and MD-2. The root-mean-square deviations (rmsd) of the C-α atoms typically provide a measure of the stability of the protein as a function of time during the course of simulation. In both MD-1 and MD-2, the rmsd initially increases up to almost 0.8 nm (Figure 2A). The high rmsd in both the simulations indicates substantial conformational change from the starting structure. In MD-1, an abrupt transition is observed near 25 ns, where the rmsd jumps from ∼0.5 to ∼0.8 nm, while in the second simulation, MD-2, the rmsd steadily increases up to 0.8 nm during the first 10 ns of the simulation. Superposition of the 100 ns averaged structures of MD-1 and MD-2 onto their starting structures (Figure 2B,C) clearly shows that the change in conformation is primarily due to motion of the bridging sheet $\beta2/\beta3$ and $\beta20/\beta21$ strands and the V3 loop, in both MD-1 (Figure 2B) and MD-2 (Figure 2C). In both simulations, the $\beta2/\beta3$ strands and V3 loops move toward each other, forming noncovalent interactions. This finding is interesting given that the V3 loop determines gp120 usage of either the CCR5 or CXC4R coreceptor[44−46] and

dx.doi.org/10.1021/bi300878d | Biochemistry 2012, 51, 7783−7793

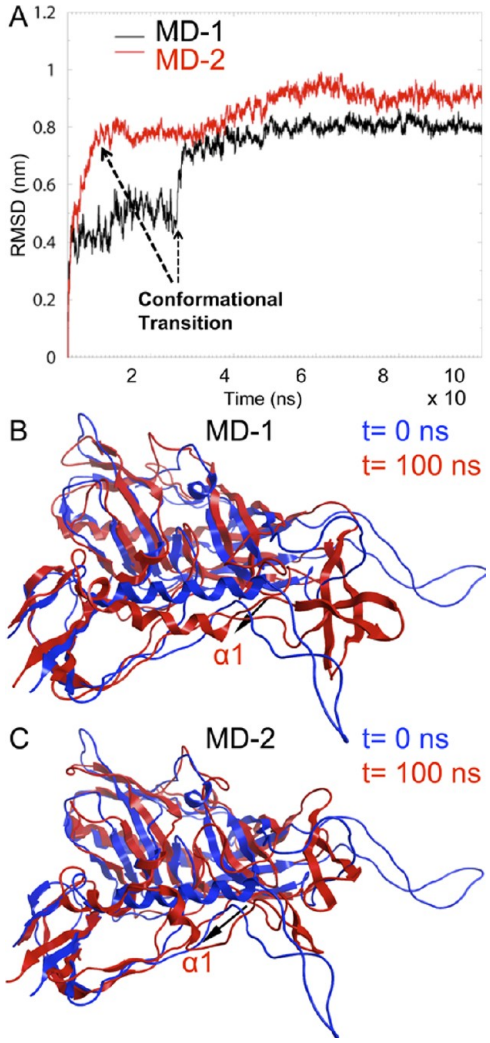

Figure 2. gp120 conformational transition. (A) The root-mean-square deviation (rmsd) for backbone C-α atoms of MD-1 (black line) and MD-2 (red line) from the initial conformation. (B) Superimposed structures of MD-1 starting structure (blue) and 100 ns structure (red) and (C) MD-2 starting structure (blue) and 100 ns structure (red). In both the simulations, the outer domain has moved less as compared to inner domain. The high rmsd at the conformational transition is due to restructuring of the $\beta2/\beta3$ and $\beta20/\beta21$ strands and the V3 loop.

further suggests that the V3 loop sequence variability may effect V3 structure and mobility as previously described.[47,67] The $\beta20/\beta21$ strand, on the other hand, moves toward W112 on inner domain helix $\alpha1$, closing off the wall of the Phe43 binding cavity between the inner and outer domains. A correlation coefficient of 0.832 in root-mean-square fluctuations (from the respective 100 ns average) (Supporting Information Figure S1) suggests remarkably similarity between the two simulations. Moreover, the 100 ns averaged structures, corresponding to the folded structure, in both MD-1 and MD-2, are also remarkably similar, with a low rmsd of 0.45 nm (Supporting Information Figure S2). In both the simulations, the topology and structure of gp120 core outer domain remain similar to the initial structure, while both the $\beta2/\beta3$ and $\beta20/\beta21$ strands and V3 loop dramatically change. Interestingly, helix $\alpha1$ in the inner domain has also shifted from the starting position in MD-1 and MD-2 and has partially lost helicity (Figure 2B,C). The transition point, observed within 30 ns in both MD-1 and MD-2 (Figure 2A), is triggered by the movement of $\beta20/\beta21$ toward the inner domain helix $\alpha1$ and the formation of a stabilizing interaction between W112 and W427 (MD-1) or W112 and Y435 (MD-2) followed by the concerted motions of $\beta2/\beta3$ and V3 loops toward (Figure 2B,C) each other.

Events Leading to Bridging Sheet Rearrangement. To assess the hierarchy of folding events, we monitored the time evolution of the minimum distances between any two atoms on residues W427 or Y435 on $\beta20/\beta21$ and W112 on inner domain helix $\alpha1$ (Figure 3A,B). These residues were considered since they form part of an aromatic cluster (W112, F210, F382,

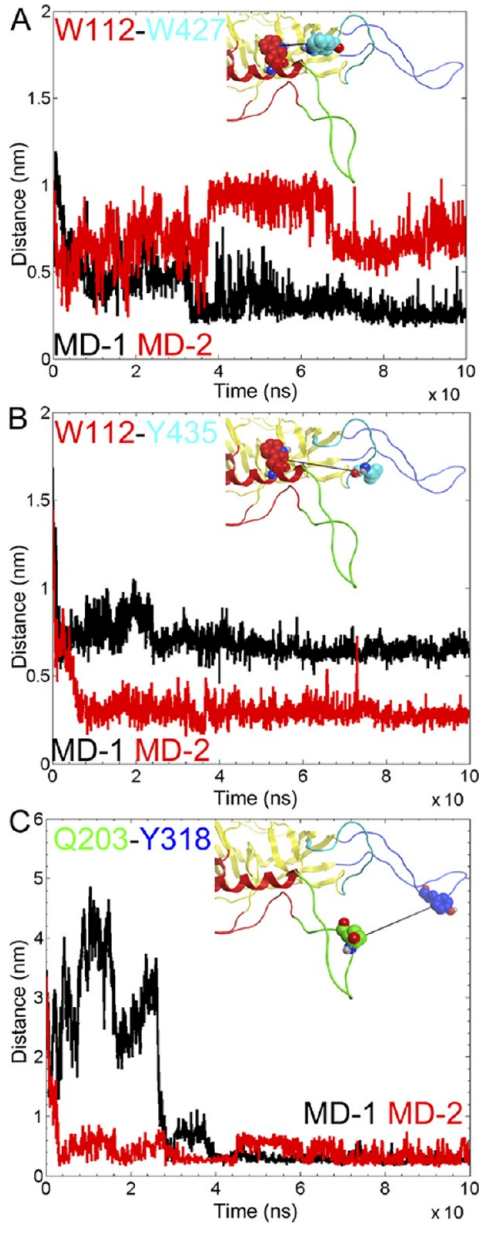

Figure 3. Monitoring $\beta2/\beta3$ and $\beta20/\beta21$ strands and the V3 loop rearrangement. (A) The minimum distances between W112 (red spheres) and W427 (cyan spheres) in MD-1 and MD-2, black and red line, respectively. (B) The minimum distances in MD-1 and MD-2 black and red line, respectively for the residue pairs, W112 (red spheres) and Y435 (cyan spheres). (C) The minimum distances in MD-1 and MD-2, black and red line, respectively, for the Q203 (green spheres) and Y318 (cyan spheres) residue pair.

dx.doi.org/10.1021/bi300878d | *Biochemistry* 2012, 51, 7783−7793

W427, Y435) that coalesces between the inner, outer, and bridging sheet upon formation of the Phe43 cavity as observed in $gp120_{CD4}$ structures. In MD-1, the minimum distance between W112 and W427 initially increases (Figure 3A, black line); however, within 10 ns this distance drops to ~0.5 nm for up to 40 ns and then finally to ~0.25 nm for the remainder of the simulation, suggesting a close interaction between W112 and W427. In MD-2 (Figure 3A, red line), residues W112 and W427 are farther apart (0.75 nm) during the first 40 ns and then later increase to ~1.0 nm, as a result of the W427 aromatic ring rotating away from W112. Closer inspection of W112 interactions with β20 indicates that in MD-2 the helix α1−β20 interaction is stabilized instead by the W112−Y435 interaction (0.25 nm) (Figure 3B, red line) maintaining the cavity like structure. In MD-1, W427 approaches W112 in a T-stacking aromatic−aromatic interaction but remains on the outer flank of W112 and the Phe43 cavity (Supporting Information, WT1_MD_movie). In the MD-2 simulation, after both W427 and Y435 form T-stacking interactions with W112, W427 then slides over the surface of W112 to settle over the top of the cavity within van der Waals interaction distance of C-β atom of S375 on the outer domain (Supporting Information, WT2_MD_movie). Thus, monitoring interactions of W112 with W427 and Y435 indicates that the β20/β21 rearranges rapidly (within 40 ns) to form close associations with inner and outer domain residues, enclosing the Phe43 cavity.

A study by Xiang et al. concluded that the V3 loop and bridging sheets assist in stabilizing the unliganded conformation of the gp120 trimer.[68] Kwon et al. further posit that $gp120_{coreE}$ exhibits an altered conformational equilibrium as a consequence of the V3 loop truncations.[38] To assess the possible role of the V3 loop in assisting bridging sheet dynamics, in the absence of a bound ligand, the interaction distance was monitored between Q203 on β2/β3 and Y318 on the V3 loop (Figure 3C). These two residues were selected because they are observed to be in close contact (less than 0.5 nm) at the end of the simulation (Supporting Information Table S1 and movies). In MD-1 (Figure 3C, black line) β2/β3 and V3 initially shift apart, and then at ~30 ns, β2/β3 and V3 move within 0.5 nm and remain associated for the duration of the simulation. In contrast, in MD-2, association between the β2/β3 and the V3 loop is seen to be formed almost instantaneously, with the two residues approaching within ~0.25 nm of each other. Analysis of the movies (Supporting Information) and the interaction plots for residue pairs W112:W427 (Figure 3A) and W112:Y435 (Figure 3B) and Q203:Y318 (Figure 3C) reveal that in both MD-1 and MD-2 the β2/β3 and β20/β21strands and V3 loop reorganize within the same time frame. The crystal structures of the unliganded $gp120_{coreE}$[38] indicate that residues in the stem of the truncated V3 loop stabilize the $gp120_{CD4}$ conformation by forming hydrogen bonds with the main-chain atoms of the β20/β21 strands. In the case of $gp120_{F105-V3}$, MD-1 and MD-2 trajectories reveal only transiently formed hydrogen bonds between V3 loop and β20/β21 strands during simulation. Thus, the rearrangement of β20/β21 in the absence of ligand in less than 40 ns is not impeded by V3 loop interaction. Nonetheless, the V3 loop closely associates with the β2/β3 throughout the simulations, likely preventing β2/β3 interaction with β20/β21. Thus, the β20/β21 strand spontaneously rearranges to enclose the Phe43 cavity via close interactions with the inner and outer domain residues.

Role of Conserved N425 in Driving Bridging Sheet Rearrangement. We next assessed interaction distances for all residues pairs between the β20/β21 strand and residues from inner domain and the outer domain within the vicinity of the Phe43 cavity. A strong interaction is defined as an interaction in which the minimum distance between any two atoms of the residue pair is less than or equal to 0.4 nm, and the distance is maintained over a period of at least 20 ns or more. The residue pairs with the strongest interactions are listed in Table 1. Both

Table 1. Distance for Strongly Interacting Residues Pairs in gp120 Crystal Structures

			distance[a] (nm)	
β20/β21	inner domain	outer domain	$gp120_{CD4}$ (1G9N)	$gp120_{F105-V3}$
K421		F382	0.309	0.190
K421		Y384	0.398	0.232
N425		V254	1.341	1.509
N425		F382	0.633	0.907
	W112	G380	0.994	0.553
W427	W112		0.324	1.023

[a]The minimum distance between any two atoms of the residue pairs.

N425 and K421 have the strongest interactions with the outer domain throughout the simulation. The inter-residue distances (N425 to W112 and N425 to F328) were monitored for MD-1 and MD-2 (Figure 4A−C). Further, inspection of the MD-1 and MD-2 trajectories reveals that N425 assists in the rearrangement of β20/β21 (Supporting Information movies). As shown in the 100 ns snapshots for MD-1 and MD-2 (Figure 4D,F), N425 rearranges to interact with F382 in the outer domain over the course of the simulation. The transition begins within the first 4 ns of the simulation, with the side chain of N425 reversing its orientation from solvent exposed to interacting with W112 on the inner domain. In the MD-1 simulation (Figure 4A, black line), N425 remains in contact with W112 (0.25 nm) for ~35 ns and then moves across the Phe43 cavity and interacts with F382 (Figure 4A, red line, and Figure 4D) and S375 in the outer domain for the remainder of the simulation. In MD-2, after brief contact (~5 ns) with W112, N425 shifts to interact with F382 for the duration of the simulation (Figure 4B red line, and Figure 4F). The N425−F382 interaction is not observed in the CD4 bound form of gp120 (for example in 1G9N); instead, N425 hydrogen bonds to E370, anchoring the bridging sheet to the outer domain in $gp120_{CD4}$ (Figure 4E and Figure S3). Interestingly, residue N425 is 75% conserved among HIV strains and is most often substituted by arginine. Furthermore, a gp120 triple mutation, I423M/N425 K/G431E, exhibits both reduced soluble CD4 and antibody 17b binding,[26] adding support to the role of N425 strand in mediating bridging sheet reorganization. Therefore, N425 appears to initiate β20/β21 rearrangement by first interacting with W112 on the inner domain and then with F382 on the outer domain. This rearrangement then positions W427 and Y435 in close proximity of W112, early on during the simulation, stabilizing β20/β21 interaction with the inner and outer domains.

The pivotal role of N425 led us to examine adjacent β20 residues (K421, N422, I423, I424, and M426) as these are all in close proximity to the outer domain in $gp120_{CD4}$. In the $gp120_{F105}$ crystal structure K421 is within interacting distance of F382 and Y384 in the outer domain (Table 1). In both MD-1 and MD-2, K421−Y384 interaction is maintained (Table 2 and Figure S4). The K421−F382 interaction is maintained in MD-2, while in MD-1 it dissipates at ~40 ns. In MD-1, the key

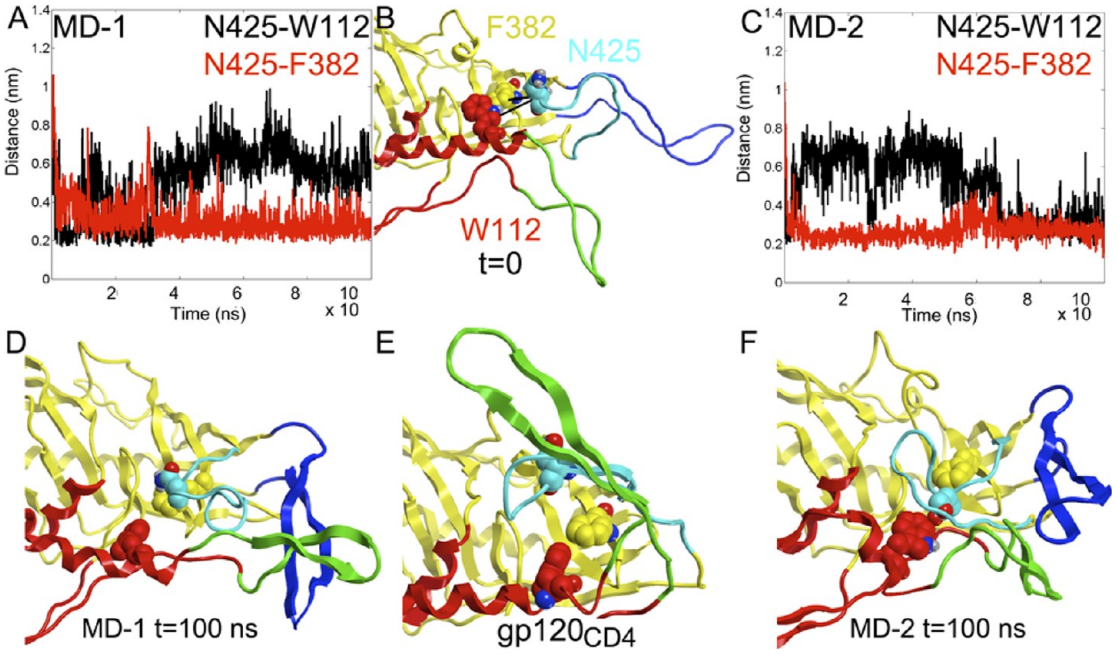

Figure 4. The role of N425 in $\beta20/\beta21$ rearrangement. (A) The minimum distances between N425 and W112 (black) and N425 and F382 (red) in MD-1 and (C) MD-2. (B) Ribbon diagram of the starting structure, in which the residue pairs whose distances were measured are highlighted: W112 (red spheres), N425 (cyan spheres), and F382 (yellow spheres). (D) The MD-1 100 ns snapshot showing the association between N425 (cyan spheres) and W112 (red spheres) and F382 (yellow spheres). (E) In $gp120_{CD4}$, X-ray structure (pdb 1G9N) of the corresponding locations of W112 (red spheres), N425 (cyan spheres), and F382 (yellow spheres) (F) The MD-2 100 ns snapshot, with the residues highlighted the same as in (D).

Table 2. Analysis of Key Interactions in MD Simulations

interactions[a]	av[b]	std dev	percent[c]	cluster1[d]	cluster2[e]
MD-1					
K421−F382	0.392	0.129	60.3	0.320	0.531
K421−Y384	0.296	0.042	100	0.202	0.308
N425−V254	0.337	0.171	85.4	0.379	0.389
N425−F382	0.311	0.104	92.2	0.267	0.422
W112−W427	0.373	0.149	74.3	0.422	0.366
W112−G380	0.843	0.122	0.05	0.657	0.829
MD-2					
K421−F382	0.199	0.020	100	0.223	0.177
K421−Y384	0.291	0.040	100	0.223	0.278
N425−V254	0.299	0.115	97.7	0.293	0.201
N425−F382	0.269	0.061	98.9	0.275	0.253
W112−W427	0.737	0.165	3.29	0.791	0.649
W112−G380	0.969	0.122	0.45	1.064	0.927

[a]The first five interactions are bridging-sheet/inner-domain interactions; the sixth is inner-domain/outer-domain interaction. [b]Minimum distance between any two atoms, averaged over 100 ns simulations. [c]Percentage time a given interaction (minimum distance between any two atoms is ≤0.45 nm) over the 100 ns period. [d]Cluster1 corresponds to clusters centered around structure, at t = 18600.0 and 34100.00 ps respectively for MD-1 and MD-2. [e]Cluster2 corresponds to clusters centered around structure, at t = 65800.00 and 86550.00 ps respectively for MD-1 and MD-2.

bridging-sheet/inner-domain interactions are all maintained over 60% of the simulation period, with an average standard deviation of 0.1 nm (Table 2). In MD-2, except for W112−W427, the remaining bridging-sheet/inner-domain key interactions are all maintained over 97% of the simulation time (Table 2) with an average standard deviation of 0.05 nm (Table 2).

Clustering analysis revealed two major clusters in MD-1 and MD-2 (Figure S5). The clustering was performed using the Jarvis−Patrick method, which uses the nearest-neighbor approach.[69] In this method, the similarity is determined using a distance metric, and the neighbors of a given structure are the closest structures within a cutoff (0.1 nm). In MD-1, the major structural difference between the two clusters is in the bridging-sheet conformation (Figure S5A,B), whereas in MD-2 a less dramatic difference is observed between the orientations of the $\beta20/\beta21$ strands (Figure S5C,D). The key bridging-sheet/inner-domain interactions excluding the W112−W427 interaction are typically weaker in cluster 2 of MD-1 (~0.4 nm) than in cluster 2 of MD-2 (~0.22 nm) (Table 2).

The next residue on $\beta20$, Q422, forms a hydrogen bond with E381 and is solvent exposed in the $gp120_{F105}$ crystal structure; however, this interaction is not maintained and Q422 remains solvent exposed throughout the MD-1 and MD-2 simulations. The behavior of neighboring $\beta20$ residues, I423 and I424, varied between the two simulations. In MD-1, I423 has close interactions with F382, while in MD-2 I424 maintains interaction with F382, suggesting both I423 and I424 have the capacity to stabilize interactions with the outer domain. Residue M426, rather than interacting with the outer domain, remains closely associated with W427 while interacting with W112 as well. To validate the importance of $\beta20$ residues in driving bridging sheet rearrangement, $gp120_{F105-V3}$ containing the I423P mutation was simulated for 100 ns. Xiang et al. introduced the I423P mutant to constrain the conformation of the bridging sheet and found that the mutant eliminated both CD4 and CD4i antibody binding.[26] Examination of the I423P trajectory demonstrates that I423P interacts with F328 and W112, blocking both the interaction of N425 with F382 and W112 and the refolding of $\beta20/\beta22$ between the inner and outer domains (Figure S6), consistent with observations

dx.doi.org/10.1021/bi300878d | Biochemistry 2012, 51, 7783−7793

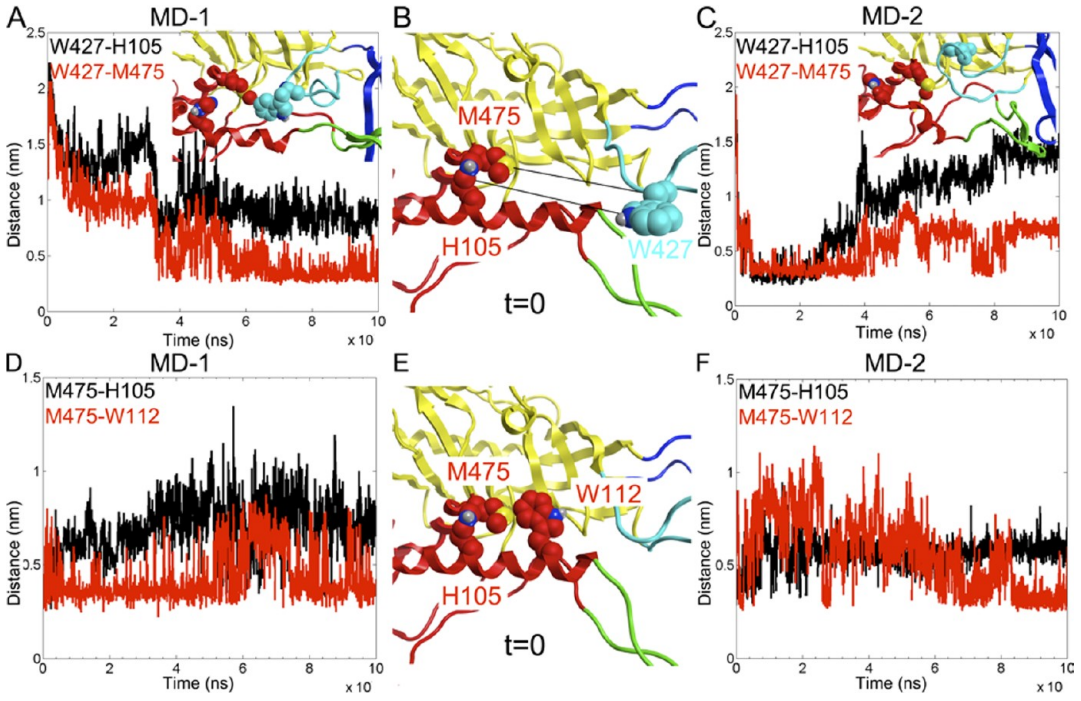

Figure 5. Inner domain stabilization of β20 residue, W427. (A) For MD-1, the minimum distances between W427 and H105 (black line) and W427 and M475 (red line). (B) Position of the residues W427 (cyan sphere) and H105 (red sphere) is indicated in the starting structure. (C) MD-2, same as in (A). (D) For MD-1, the minimum distances between M475 and H105 (black line) and M475 and W112 (red line). (E) Position of the residues M475, H105, and W112 (red spheres) is indicated in the starting structure. (F) MD-2, same as in (D).

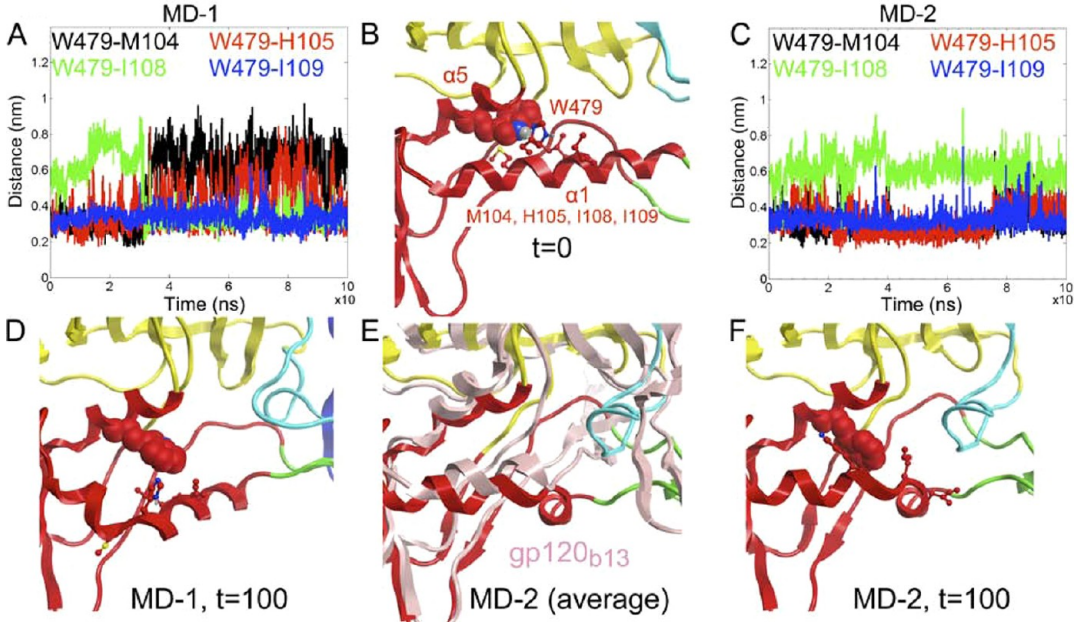

Figure 6. Shifts in inner domain helix α1. (A) For MD-1, the minimum distances between W479 and M104 (black line), W479 and H105 (red line), W479 and I108 (green line), and W479 and I109 (blue line). (B) In the starting structure, the distances between residues W479 (red spheres) and residues M104, H105, I108, and I109 (ball and stick) are highlighted. (C) MD-2 same as in (A). (D) The MD-1, 100 ns snapshot showing the kink that develops in helix α1 near H105. (E) Comparison of MD-2 and the antibody b13 bound gp120 conformation ($gp120_{b13}$) (pdb 2IDY) (pink ribbon). The loss of helicity at I108 is also apparent. (F) The MD-2, 100 ns snapshot showing the kink and loss of helicity in helix α1 around I108.

reported by Liu et al.[55] Thus, we posit that the β20/β21 strands initiate gp120 conformational change that leads to a CD4 binding competent conformation and that there is a natural propensity of the β20/β21 to reside between the inner and outer domains in the preformed Phe43 cavity. The finding that β20/β21 reorients between the inner and outer domain is generally consistent with the conformation exhibited by β20/β21 in the only crystal of unliganded gp120, from SIV (Figure S7), and suggests that β20/β21 has a tendency to adopt this conformation. The results of the simulations are further supported by experiment: mutant gp120 envelope proteins containing K421D, N422L, I423S, or I424S on β20 reduced

dx.doi.org/10.1021/bi300878d | *Biochemistry* 2012, 51, 7783−7793

binding to both soluble CD4 and CCR5,[68] and deletion of both the β20/β21 strands enhances both F105 and b12 antibody binding to gp120, suggesting a reduction of steric hindrance with its removal.[70] As the initial distance between N425 and W112 on helix α1 is 11.2 Å, a longer-range electrostatic interaction as noted by Kwong et al. may be triggering the rearrangement.[28]

Inner Domain Conformational Changes. The inner domain has been described as containing three structurally mobile layers, comprised of helix α0, helix α1, and helix α5[31] (we note that helix α0 is not observed in the $gp120_{F105}$ crystal structure). Interestingly, helix α1 is partially unfolded in the b13−gp120 and completely unfolded in the b12−gp120 cocrystal structures.[29,32] When comparing the position of helix α1 and helix α5 in $gp120_{F105}$ versus $gp120_{CD4}$, the two helices are further apart in the $gp120_{CD4}$, implying that the helix α1 and α5 shift relative to each other in order to accommodate the formation of the bridging sheet and the Phe43 cavity. Furthermore, previous computational analysis posited that H105 on helix α1 and M475 on the tip of helix α5 behave like a hinge region, stabilizing interactions with the bridging sheet.[49] Hence, we monitored the distances between W427 on β20/β21 and helices α1 (W112) and α5 (M475). The distance plot between W427−M475 indicates that W427 moves from 2.0 nm to within 0.5 nm of M475, in less than 40 ns in both MD-1 and MD-2 (Figure 5A−C, red line). Interaction between W427 and H105 on helix α1 is weaker for both MD-1 and MD-2 (Figure 5A−C, black line). The distances between M475 and H105 or W112 as an indicator of helix α1 and α5 interaction (Figure 5D−F) indicates that in MD-1 M475 maintains close interaction with W112 (∼0.25 nm) and no interaction with H105. On the other hand, in MD-2, M475 maintains steady interactions with H105 (∼0.5−0.6 nm) while the distance between M475 and W112 fluctuates. We further analyzed the interaction of residue W479 on helix α5 with residues, M104, H105, I108, and I109, on helix α1 to assess the relative motions of these two layers of the inner domain. As shown in Figure 6A−C for MD-1 and MD-2, the strongest interaction occurs between W479 and I109 (blue line), with either H105 (MD-1, red line, Figure 6A) or I108 (MD-2, green line, Figure 6B), providing additional stability between helix α1 and helix α5. Interestingly, these residues are associated much more closely in simulations of small ligand bound (NBD) or CD4 bound $gp120_{CD4}$ (GCD2) compared to the unliganded $gp120_{CD4}$ (GPO3)[49] (Figure S8).

The average distances between N-terminus and C-terminus of helix α1 with the C-terminus and N-terminus of helix α5 are ∼0.75 and ∼1.57 nm, respectively. Closer inspection indicates that a kink develops in helix α1 at M104 and H105 in MD-1 and MD-2, respectively, as early as 40 ns (Figure 6D,F). Thus, the C-terminal portion of helix α1 pivots away from the outer domain while the N-terminal portion remains more closely associated with the inner domain β-sandwich and helix α5 (Figure 6D,F). In fact, the structure of helix α1 as exhibited in the average structure of MD-2 resembles that observed in the b13−gp120 complex (Figure 6E). As expected, helix α5 in MD-1 and MD-2 maintains the same position as observed in $gp120_{CD4}$ (rmsd 0.19 and 1.6 nm) and $gp120_{F105}$ (rmsd 0.25 and 0.25 nm) crystal structures. Thus, the tight interaction between M475 and W479 on helix α5 and H105, I108, and I109 on helix α1 anchors the N-terminus region of the helix α1 while the C-terminus portion of helix α1 pivots away from the outer domain, permitting the β20/β21 strands to wedge between the inner and outer domains. Since a hydrogen bond is observed between E102 and R476 in $gp120_{CD4}$ crystal structure and the distance between E102 and R476 or R480 side chains is less than 0.4 nm in $gp120_{F105-V3}$, we also examined the electrostatic interactions between E102 (helix α1) and R476 or R480 (helix α5). This hydrogen bond or salt bridge does not form between E102 and R476 or R480 side chains in either MD-1 or MD-2. Comparison of 100 ns simulations of GPO3, NBD, and GCD2 indicates that stabilizing E102 and R476 or R480 side-chain interactions are maintained (Figure S9). Thus, in the unliganded form, the majority of the interactions between helix α1 and helix α5 are hydrophobic in nature, although weak electrostatic interactions also form between E102 and R476 or R480.

CONCLUSIONS

In this study we hypothesized that the extended β2/β3 and β20/β21 arrangement as exhibited in the antibody F105−gp120 complex represents one potential conformation of the metastable unliganded gp120 monomer for study of gp120 conformational change. The two 100 ns MD simulations demonstrate remarkably similar results with a conformational transition occurring within the first 30 ns. The transition commences with β20/β21 strand reorienting from an extended conformation exhibited in the $gp120_{F105}$ crystal structure to a folded conformation lying between the inner and outer domains, reminiscent of its position observed in $gp120_{CD4}$. Within the first 4 ns, residue N425 on β20 reorients by interacting with W112 before settling against the F382 in the outer domain positioning β20/β21 residues W427 or Y435 to interact with W112 on helix α1. The conformational transition was not observed when simulating a β20/β21 constraining mutant, I423P. The β2/β3 and the V3 loop also reorganize by folding over the β20/β21 in the simulated unliganded form of $gp120_{F105-V3}$. The rearrangement of the β20/β21 was accompanied by unwinding of helix α1 which also pivots about the N-terminus. The β20/β21 once refolded remains between the inner and outer domain for the entire 100 ns simulation period, even in the absence of a ligand. Thus, the folding of β20/β21 encloses one face of the preformed Phe43 cavity and is stabilized by interactions maintained between residues on both inner domain and outer domain.

Previous dogma held that CD4 or small molecule binding induces gp120 conformational transition from an unstructured form to the $gp120_{CD4}$ form. However, the recent crystal structure of the unliganded gp120[38] indicates that $gp120_{coreE}$ spontaneously adopts the CD4 bound conformation when not restricted by the presence of the V1, V2, and V3 variable loops. In our studies the presence of the V3 loop did not constrain the conformational rearrangement of the β20/β21 strands. However, the V3 loop formed strong interactions with the β2/β3 preventing the formation of the four-stranded antiparallel bridging sheet observed in $gp120_{CD4}$. The propensity for V3 loop reorganization to interact with the β2/β3 strand during MD simulation is consistent with V3 determinants of coreceptor usage[45,46] and the sensitivity of V3 sequence in eliciting humoral immunity.[71] The previously reported charge dependent mobility of the V3 loop as observed in MD simulation of $gp120_{CD4}$[47] is also consistent with the mobility of the loop observed in MD simulations of $gp120_{F105}$. We conclude from the simulations reported herein that the β20/β21, in unliganded gp120, has a natural propensity to adopt a conformation between the inner and outer domain.

This conclusion is consistent with the position of the β20/β21, as observed in the SIV structure[40] and as suggested by mutant data reported by Finzi et al.[41] and others.[26,68,70] Experimentally, we suggest probing the binding affinity of small molecules inhibitors[72] that display varied thermodynamic signatures in full-length gp120 containing the N425 mutant to further explore the role of β20/β21 in mediating gp120 conformational equilibrium. Moreover, the insights provided herein should be helpful in developing strategies to entrap unproductive conformations of gp120 in its unliganded form as a means of preventing HIV-1 entry.

■ ASSOCIATED CONTENT

Ⓢ Supporting Information

Figures S1−S9 and MD movies. This material is available free of charge via the Internet at http://pubs.acs.org.

■ AUTHOR INFORMATION

Corresponding Author

*E-mail ihs2@pitt.edu.

Funding

I.H.S. acknowledges NIH for support (R01LM007994-06). This work was supported by a grant from the National Institutes of Health GM56550 (J.L.).

Notes

The authors declare no competing financial interest.

■ ACKNOWLEDGMENTS

The authors appreciate the useful suggestions and discussions with Arne Schon, Navid Madani, and Ivet Bahar. Support from NIH grant R01LM007994-06 to Ivet Bahar's lab is gratefully acknowledged by I.H.S. This work was supported by a grant from the National Institutes of Health GM56550 (J.L.).

■ ABBREVIATIONS

MD, molecular dynamics; HIV-1, human immunodeficiency virus, l; rmsf, root-mean-square fluctuations; rmsd, root-mean-square deviations; $gp120_{CD4}$, CD4 bound conformation of gp120; $gp120_{coreE}$, gp120 extended core; $gp120_{core}$, truncated core gp120; $gp120_{F105}$, antibody F105 bound $gp120_{core}$ complex; $gp120_{F105-V3}$, $gp120_{F105}$, antibody F105 bound $gp120_{core}$ complex with a grafted V3 loop.

■ REFERENCES

(1) Barre-Sinoussi, F., Chermann, J. C., Rey, F., Nugeyre, M. T., Chamaret, S., Gruest, J., Dauguet, C., Axler-Blin, C., Vezinet-Brun, F., Rouzioux, C., Rozenbaum, W., and Montagnier, L. (1983) Isolation of a T-lymphotropic retrovirus from a patient at risk for acquired immune deficiency syndrome (AIDS). *Science 220*, 868−871.

(2) Gallo, R. C., Salahuddin, S. Z., Popovic, M., Shearer, G. M., Kaplan, M., Haynes, B. F., Palker, T. J., Redfield, R., Oleske, J., Safai, B., et al. (1984) Frequent detection and isolation of cytopathic retroviruses (HTLV-III) from patients with AIDS and at risk for AID. *Science 224*, 500−503.

(3) Dalgleish, A. G., Beverley, P. C., Clapham, P. R., Crawford, D. H., Greaves, M. F., and Weiss, R. A. (1984) The CD4 (T4) antigen is an essential component of the receptor for the AIDS retrovirus. *Nature 312*, 763−767.

(4) McDougal, J. S., Kennedy, M. S., Sligh, J. M., Cort, S. P., Mawle, A., and Nicholson, J. K. (1986) Binding of HTLV-III/LAV to T4+ T cells by a complex of the 110K viral protein and the T4 molecule. *Science*, 231.

(5) Klatzmann, D., Champagne, E., Chamaret, S., Gruest, J., Guetard, D., Hercend, T., Gluckman, J. C., and Montagnier, L. (1984) T-lymphocyte T4 molecule behaves as the receptor for human retrovirus LAV. *Nature 314*, 767−768.

(6) Wyatt, R., and Sodroski, J. (1998) The HIV-1 envelope glycoproteins fusogens antigens and immunogens. *Science 280*, 1884−1888.

(7) Ugolini, S., Moulard, M., Mondor, I., Barois, N., Demandolx, D., Hoxie, J., Brelot, A., Alizon, M., Davoust, J., and Sattentau, Q. J. (1997) HIV-1 gp120 induces an association between CD4 and the chemokine receptor CXCR4. *J Immunol. 159*, 3000−3008.

(8) Blacklow, S. C., Lu, M., and Kim, P. S. (1995) A trimeric subdomain of the simian immunodeficiency virus envelope glycoprotein. *Biochemistry 34*, 14955−14962.

(9) Lu, M., Blacklow, S. C., and Kim, P. S. (1995) A trimeric structural domain of the HIV-1 transmembrane glycoprotein. *Nat. Struct. Biol. 2*, 1075−1082.

(10) Kowalski, M., Potz, J., Basiripour, L., Dorfman, T., Goh, W. C., Terwilliger, E., Dayton, A., Rosen, C., Haseltine, W., and Sodroski, J. (1987) Functional regions of the envelope glycoprotein of human immunodeficiency virus type 1. *Science 237*, 1351−1355.

(11) Dragic, T., Litwin, V., Allaway, G. P., Martin, S. R., Huang, Y., Nagashima, K. A., Cayanan, C., Maddon, P. J., Koup, R. A., Moore, J. P., and Paxton, W. A. (1996) HIV-1 entry into CD4+ cells is mediated by the chemokine receptor CC-CKR-5. *Nature 381*, 667−673.

(12) Sattentau, Q. J., and Moore, J. P. (1991) Conformational changes induced in the human immunodeficiency virus envelope glycoprotein by soluble CD4 binding. *J. Exp. Med. 174*, 407−415.

(13) Sattentau, Q. J., Moore, J. P., Vignaux, F., Traincard, F., and Poignard, P. (1993) Conformational changes induced in the envelope glycoproteins of the human and simian immunodeficiency viruses by soluble receptor binding. *J. Virol. 67*, 7383−7393.

(14) Wu, L., Gerard, N. P., Wyatt, R., Choe, H., Parolin, C., Ruffing, N., Borsetti, A., Cardoso, A. A., Desjardin, E., Newman, W., Gerard, C., and Sodroski, J. (1996) CD4-induced interaction of primary HIV-1 gp120 glycoproteins with the chemokine receptor CCR-5. *Nature*, 384.

(15) Choe, H., Farzan, M., Sun, Y., Sullivan, N., Rollins, B., Ponath, P. D., Wu, L., Mackay, C. R., LaRosa, G., Newman, W., Gerard, N., Gerard, C., and Sodroski, J. (1996) The beta-chemokine receptors CCR3 and CCR5 facilitate infection by primary HIV-1 isolates. *Cell 85*, 1135−1148.

(16) Deng, H., Liu, R., Ellmeier, W., Choe, S., Unutmaz, D., Burkhart, M., Di Marzio, P., Marmon, S., Sutton, R. E., Hill, C. M., Davis, C. B., Peiper, S. C., Schall, T. J., Littman, D. R., and Landau, N. R. (1996) Identification of a major co-receptor for primary isolates of HIV-1. *Nature 381*, 661−666.

(17) Doranz, B. J., Rucker, J., Yi, Y., Smyth, R. J., Samson, M., Peiper, S. C., Parmentier, M., Collman, R. G., and Doms, R. W. (1996) A dual-tropic primary HIV-1 isolate that uses fusin and the beta-chemokine receptors CKR-5, CKR-3, and CKR-2b as fusion cofactors. *Cell 85*, 1149−1158.

(18) Bosch, M. L., Earl, P. L., Fargnoli, K., Picciafuoco, S., Giombini, F., Wong-Staal, F., and Franchini, G. (1989) Identification of the fusion peptide of primate immunodeficiency viruses. *Science 244*, 694−697.

(19) Brasseur, R., Cornet, B., Burny, A., Vandenbranden, M., and Ruysschaert, J. M. (1988) Mode of insertion into a lipid membrane of the N-terminal HIV gp41 peptide segment. *AIDS Res. Hum. Retroviruses 4*, 83−90.

(20) Helseth, E., Olshevsky, U., Gabuzda, D., Ardman, B., Haseltine, W., and Sodroski, J. (1990) Changes in the transmembrane region of the human immunodeficiency virus type 1 gp41 envelope glycoprotein affect membrane fusion. *J. Virol. 64*, 6314−6318.

(21) Myszka, D. G., Sweet, R. W., Hensley, P., Brigham-Burke, M., Kwong, P. D., Hendrickson, W. A., Wyatt, R., Sodroski, J., and Doyle, M. L. (2000) Energetics of the HIV gp120-CD4 binding reaction. *Proc. Natl. Acad. Sci. U. S. A. 97*, 9026−9031.

(22) Dey, B., Pancera, M., Svehla, K., Shu, Y., Xiang, S. H., Vainshtein, J., Li, Y., Sodroski, J., Kwong, P. D., Mascola, J. R., and Wyatt, R. (2007) Characterization of human immunodeficiency virus type 1 monomeric and trimeric gp120 glycoproteins stabilized in the

CD4-bound state: antigenicity, biophysics, and immunogenicity. *J. Virol. 81*, 5579−5593.
(23) Kwong, P. D., Wyatt, R., Desjardins, E., Robinson, J., Culp, J. S., Hellmig, B. D., Sweet, R. W., Sodroski, J., and Hendrickson, W. A. (1999) Probability analysis of variational crystallization and its application to gp120, the exterior envelope glycoprotein of type 1 human immunodeficiency virus (HIV-1). *J. Biol. Chem. 274*, 4115−4123.
(24) Schon, A., Madani, N., Klein, J. C., Hubicki, A., Ng, D., Yang, X., Smith, A. B., 3rd, Sodroski, J., and Freire, E. (2006) Thermodynamics of binding of a low-molecular-weight CD4 mimetic to HIV-1 gp120. *Biochemistry 45*, 10973−10980.
(25) Dey, B., Svehla, K., Xu, L., Wycuff, D., Zhou, T., Voss, G., Phogat, A., Chakrabarti, B. K., Li, Y., Shaw, G., Kwong, P. D., Nabel, G. J., Mascola, J. R., and Wyatt, R. T. (2009) Structure-based stabilization of HIV-1 gp120 enhances humoral immune responses to the induced co-receptor binding site. *PLoS Pathog. 5*, e1000445.
(26) Xiang, S. H., Kwong, P. D., Gupta, R., Rizzuto, C. D., Casper, D. J., Wyatt, R., Wang, L., Hendrickson, W. A., Doyle, M. L., and Sodroski, J. (2002) Mutagenic stabilization and/or disruption of a CD4-bound state reveals distinct conformations of the human immunodeficiency virus type 1 gp120 envelope glycoprotein. *J. Virol. 76*, 9888−9899.
(27) Kwong, P. D., Wyatt, R., Majeed, S., Robinson, J., Sweet, R. W., Sodroski, J., and Hendrickson, W. A. (2000) Structures of HIV-1 gp120 envelope glycoproteins from laboratory-adapted and primary isolates. *Struct. Fold. Des. 8*, 1329−1339.
(28) Kwong, P. D., Wyatt, R., Robinson, J., Sweet, R. W., Sodroski, J., and Hendrickson, W. A. (1998) Structure of an HIV gp120 envelope glycoprotein in complex with the CD4 receptor and a neutralizing human antibody. *Nature 393*, 648−659.
(29) Zhou, T., Xu, L., Dey, B., Hessell, A. J., Van Ryk, D., Xiang, S. H., Yang, X., Zhang, M. Y., Zwick, M. B., Arthos, J., Burton, D. R., Dimitrov, D. S., Sodroski, J., Wyatt, R., Nabel, G. J., and Kwong, P. D. (2007) Structural definition of a conserved neutralization epitope on HIV-1 gp120. *Nature 445*, 732−737.
(30) Diskin, R., Marcovecchio, P. M., and Bjorkman, P. J. (2010) Structure of a clade C HIV-1 gp120 bound to CD4 and CD4-induced antibody reveals anti-CD4 polyreactivity. *Nat. Struct. Mol. Biol. 17*, 608−613.
(31) Pancera, M., Majeed, S., Ban, Y. E., Chen, L., Huang, C. C., Kong, L., Kwon, Y. D., Stuckey, J., Zhou, T., Robinson, J. E., Schief, W. R., Sodroski, J., Wyatt, R., and Kwong, P. D. (2010) Structure of HIV-1 gp120 with gp41-interactive region reveals layered envelope architecture and basis of conformational mobility. *Proc. Natl. Acad. Sci. U. S. A. 107*, 1166−1171.
(32) Chen, L., Kwon, Y. D., Zhou, T., Wu, X., O'Dell, S., Cavacini, L., Hessell, A. J., Pancera, M., Tang, M., Xu, L., Yang, Z.-Y., Zhang, M.-Y., Arthos, J., Burton, D. R., Dimitrov, D. S., Nabel, G. J., Posner, M. R., Sodroski, J., Wyatt, R., Mascola, J. R., and Kwong, P. D. (2009) Structural Basis of Immune Evasion at the Site of CD4 Attachment on HIV-1 gp120. *Science 326*, 1123−1127.
(33) Huang, C.-C., Lam, S. N., Acharya, P., Tang, M., Xiang, S.-H., Shahzad-ul Hussan, S., Stanfield, R. L., Robinson, S., Sodroski, J., Wilson, I. A., Wyatt, R., Bewley, C. A., and Kwong, P. D. (2007) Structures of the CCR5 N Terminus and of a Tyrosine-Sulfated Antibody with HIV-1 gp120 and CD4. *Science 319*, 1930−1934.
(34) Zhou, T., Georgiev, I., Wu, X., Yang, Z. Y., Dai, K., Finzi, A., Kwon, Y. D., Scheid, J. F., Shi, W., Xu, L., Yang, Y., Zhu, J., Nussenzweig, M. C., Sodroski, J., Shapiro, L., Nabel, G. J., Mascola, J. R., and Kwong, P. D. (2010) Structural basis for broad and potent neutralization of HIV-1 by antibody VRC01. *Science 329*, 811−817.
(35) Wu, X., Zhou, T., Zhu, J., Zhang, B., Georgiev, I., Wang, C., Chen, X., Longo, N. S., Louder, M., McKee, K., O'Dell, S., Perfetto, S., Schmidt, S. D., Shi, W., Wu, L., Yang, Y., Yang, Z. Y., Yang, Z., Zhang, Z., Bonsignori, M., Crump, J. A., Kapiga, S. H., Sam, N. E., Haynes, B. F., Simek, M., Burton, D. R., Koff, W. C., Doria-Rose, N. A., Connors, M., Mullikin, J. C., Nabel, G. J., Roederer, M., Shapiro, L., Kwong, P. D., and Mascola, J. R. (2011) Focused evolution of HIV-1 neutralizing antibodies revealed by structures and deep sequencing. *Science 333*, 1593−1602.
(36) Huang, C. C., Stricher, F., Martin, L., Decker, J. M., Majeed, S., Barthe, P., Hendrickson, W. A., Robinson, J., Roumestand, C., Sodroski, J., Wyatt, R., Shaw, G. M., Vita, C., and Kwong, P. D. (2005) Scorpion-toxin mimics of CD4 in complex with human immunodeficiency virus gp120 crystal structures, molecular mimicry, and neutralization breadth. *Structure 13*, 755−768.
(37) Stricher, F., Huang, C.-c., Descours, A., Duquesnoy, S., Combes, O., Decker, J. M., Do Kwon, Y., Lusso, P., Shaw, G. M., Vita, C., Kwong, P. D., and Martin, L. (2008) Combinatorial Optimization of a CD4-Mimetic Miniprotein and Cocrystal Structures with HIV-1 gp120 Envelope Glycoprotein. *J. Mol. Biol. 382*, 510−524.
(38) Kwon, Y. D., Finzi, A., Wu, X., Dogo-isonagie, C., Lee, L. K., Moore, L. R., Schmidt, S. R., Stuckey, J., Yang, Y., Zhou, T., Zhu, J., Vicice, D. A., Debnath, A. K., Shapiro, L., Bewley, C. A., Mascola, J. R., Sodroski, J., and Kwong, P. D. (2012) Unliganded HIV-1 gp120 Structures Reveal Propensity of Core to Assume the CD4-Bound Conformation with Regulation by Quaternary Interactions and Variable Loops. *Proc. Natl. Acad. Sci. U. S. A. 109*, 5663−5668.
(39) LaLonde, J. M., Kwon, Y. D., Jones, D. M., Sun, A. W., Courter, J. R., Soeta, T., Kobayashi, T., Princiotto, A. M., Wu, X., Schön, A., Freire, E., Kwong, P. D., Mascola, J. R., Sodroski, J., Madani, N., and Smith, A. B., III (2012) Dual Hot Spot Structure-Based Design, Synthesis and Characterization of Small-Molecule HIV-1 Entry Inhibitors. *J. Med. Chem. 55*, 4382−4396.
(40) Chen, B., Vogan, E. M., Gong, H., Skehel, J. J., Wiley, D. C., and Harrison, S. C. (2005) Structure of an unliganded simian immunodeficiency virus gp120 core. *Nature 433*, 834−841.
(41) Finzi, A., Xiang, S. H., Pacheco, B., Wang, L., Haight, J., Kassa, A., Danek, B., Pancera, M., Kwong, P. D., and Sodroski, J. (2010) Topological layers in the HIV-1 gp120 inner domain regulate gp41 interaction and CD4-triggered conformational transitions. *Mol. Cell 37*, 656−67.
(42) Huang, C. C., Tang, M., Zhang, M. Y., Majeed, S., Montabana, E., Stanfield, R. L., Dimitrov, D. S., Korber, B., Sodroski, J., Wilson, I. A., Wyatt, R., and Kwong, P. D. (2005) Structure of a V3-containing HIV-1 gp120 core. *Science 310*, 1025−1028.
(43) Huang, C.-C., Venturi, M., Moore, M. J., Phogat, S., Zhang, M.-Y., Hendrickson, W. A., Robinson, J., Sodroski, J., Wyatt, R., Choe, H., Farzan, M., and Kwong, P. D. (2004) Structural basis of tyrosine sulfation and VH-gene usage in antibodies that recognize the HIV type 1 coreceptor-binding site on gp120. *Proc. Natl. Acad. Sci. U. S. A. 101*, 2706−2711.
(44) Hartley, O., Klasse, P. J., Sattentau, Q. J., and Moore, J. P. (2005) V3: HIV's switch-hitter. *AIDS Res. Hum. Retroviruses 21*, 171−89.
(45) Cann, A. J., Churcher, M. J., Boyd, M., O'Brien, W., Zhao, J. Q., Zack, J., and Chen, I. S. (1992) The region of the envelope gene of human immunodeficiency virus type 1 responsible for determination of cell tropism. *J. Virol. 66*, 305−9.
(46) Westervelt, P., Trowbridge, D. B., Epstein, L. G., Blumberg, B. M., Li, Y., Hahn, B. H., Shaw, G. M., Price, R. W., and Ratner, L. (1992) Macrophage tropism determinants of human immunodeficiency virus type 1 in vivo. *J. Virol. 66*, 2577−82.
(47) Yokoyama, M., Naganawa, S., Yoshimura, K., Matsushita, S., and Sato, H. (2012) Structural Dynamics of HIV-1 Envelope Gp120 Outer Domain with V3 Loop. *PLoS One 7*, e37530 Epub 2012 May 18.
(48) Tan, H., and Rader, A. J. (2009) Identification of putative, stable binding regions through flexibility analysis of HIV-1 gp120. *Proteins: Struct., Func., Bionf. 74*, 881−894.
(49) Shrivastava, I., and LaLonde, J. M. (2010) Fluctuation dynamics analysis of gp120 envelope protein reveals a topologically based communication network. *Proteins: Struct., Funct., Bioinf. 78*, 2935−2949.
(50) Abrams, C. F., and Vanden-Eijnden, E. (2010) Large-scale conformational sampling of proteins using temperature-accelerated molecular dynamics. *Proc. Natl. Acad. Sci. U. S. A. 107*, 4961−4966.

(51) Hsu, S.-T. D., and Bonvin, A. M. J. J. (2004) Atomic insight into the CD4 binding-induced conformational changes in HIV-1 gp120. *Proteins: Struct., Funct., Bioinf. 55*, 582−593.
(52) Hsu, S.-T. D., Peter, D., van Gunsteren, W. F., and Bonvin, A. M. J. J. (2005) Entropy Calculation of HIV-1 Env gp120, its Receptor CD4, and their Complex: An Analysis of Configurational Entropy Changes upon Complexation. *Biophys. J. 88*, 14−24.
(53) Da, L.-T., Quan, J.-M., and Wu, Y. D. (2009) Understanding of the Brdiging Sheet Formation of HIV-1 Glycoprotein gp120. *J. Phys. Chem. B 113*, 14536−14543.
(54) Pan, Y., Ma, B., Keskin, O., and Nussinov, R. (2004) Characterization of the conformational state and flexibility of HIV-1 glycoprotein gp120 core domain. *J. Biol. Chem. 279*, 30523−30530.
(55) Liu, S. Q., Liu, S. X., and Fu, Y. X. (2008) Molecular motions of human HIV-1 gp120 envelope glycoproteins. *J Mol. Model. 14*, 857−870.
(56) Pan, Y., Ma, B., and Nussinov, R. (2005) CD4 binding partially locks the bridging sheet in gp120 but leaves the beta2/3 strands flexible. *J. Mol. Biol. 350*, 514−527.
(57) Shrivastava, I., and Lalonde, J. M. (2011) Enhanced Dynamics of HIV gp120 Glycoprotein by Small Molecule Binding. *Biochemistry 50*, 4173−4183.
(58) Molecular Operating Environment (MOE), 2011.10; Chemical Computing Group Inc., 1010 Sherbooke St. West, Suite #910, Montreal, QC, Canada, H3A 2R7, 2011.
(59) Lovell, S. C., Davis, I. W., Arendall, W. B., III, de Bakker, P. I., Word, J. M., Prisant, M. G., Richardson, J. S., and Richardson, D. C. (2003) Structure validation by Calpha geometry: phi,psi and Cbeta deviation. *Proteins 50*, 437−450.
(60) Word, J., Lovell, S., Richardson, J., and Richardson, D. (1999) Asparagine and glutamine: Using hydrogen atom contacts in the choice of side-chain amide orientation. *J. Mol. Biol. 285*, 1735−1747.
(61) Jorgensen, W. L., Maxwell, D. S., and Tirado-Rives, J. (1996) Development and testing of the OPLS all-atom force field on conformational energetics and properties of organic liquids. *J. Am. Chem. Soc. 117*, 11225−11236.
(62) Lindahl, E. H. B., and van der Spoel, D. (2001) GROMACS 30 A package for molecular simulation and trajectory analysis. *J. Mol. Model. 7*, 306−317.
(63) Van der Spoel, E., Lindahl, B., Hess, G., Mark Groenhof, A. E., and Berendsen, H. J. C. (2005) GROMACS Fast Flexible and Free. *J. Comput. Chem. 26*, 1701−1718.
(64) Berendsen, H. J. C., Grigera, J. R., Straatsma, P. R., Berendsen, H. J. C., Grigera, J. R., and Straatsma, P. R. (1987) *J. Phys. Chem. 91*, 6269−6271.
(65) Hess, B., Bekker, H., Berendsen, H. J. C., and Fraaije, J. (1997) LINCS: A linear constraint solver for molecular simulations. *J. Comput. Chem. 18*, 1463−1472.
(66) Essmann, U., Perera, L., Berkowitz, M. L., Darden, T., Lee, H., and Pedersen, L. G. (1995) A smooth particle mesh ewald method. *J. Chem. Phys. 103*, 8577−8593.
(67) Andrianov, A. M., Anishchenko, I. V., and Tuzikov, A. V. (2011) Discovery of novel promising targets for anti-AIDS drug developments by computer modeling: application to the HIV-1 gp120 V3 loop. *J. Chem. Inf. Model. 51*, 2760−7 Epub 2011 Sep 22.
(68) Xiang, S. H., Finzi, A., Pacheco, B., Alexander, K., Yuan, W., Rizzuto, C., Huang, C. C., Kwong, P. D., and Sodroski, J. (2010) A V3 loop-dependent gp120 element disrupted by CD4 binding stabilizes the human immunodeficiency virus envelope glycoprotein trimer. *J. Virol. 84*, 3147−3161.
(69) Jarvis, R. A., and Patrick, E. A. (1973) Clustering Using a Similarity Measure Based on Shared Near Neighbors. *IEEE Trans. Comput. C22*, 1025−1034.
(70) Berkower, I., Patel, C., Ni, Y., Virnik, K., Xiang, Z., and Spadaccini, A. (2008) Targeted deletion in the beta20-beta21 loop of HIV envelope glycoprotein gp120 exposes the CD4 binding site for antibody binding. *Virology 377*, 330−8 Epub 2008 Jun 2.
(71) Goudsmit, J., Debouck, C., Meloen, R. H., Smit, L., Bakker, M., Asher, D. M., Wolff, A. V., Gibbs, C. J., Jr., and Gajdusek, D. C. (1988) Human immunodeficiency virus type 1 neutralization epitope with conserved architecture elicits early type-specific antibodies in experimentally infected chimpanzees. *Proc. Natl. Acad. Sci. U. S. A. 85*, 4478−4482.
(72) Schön, A., Madani, N., Smith, I., LaLonde, A. B., Freire, J. M., and Some Drug, E. (2011) Properties are Dependent on Thermodynamic Signature. *Chem. Biol. Drug Des. 77*, 161−165.